Doubly heavy hadron production in ultraperipheral collision

Hao Yang[1,‡] Jun Jiang[2,*] and Bingwei Long[1,3,†]

[1]*College of Physics, Sichuan University, Chengdu, Sichuan 610065, China*
[2]*School of Physics, Shandong University, Jinan, Shandong 250100, China*
[3]*Southern Center for Nuclear-Science Theory (SCNT), Institute of Modern Physics,
Chinese Academy of Sciences, Huizhou 516000, Guangdong, China*

We study the double heavy baryon $\Xi_{QQ'}$ and tetraquark T_{QQ} production through photon-photon and photon-gluon fusion via ultraperipheral collisions at the LHC and Future Circular Collider (FCC) within the framework of nonrelativistic QCD factorization formalism. Various ion-ion collisions are taken into account, two $cc(bb)$-diquark configurations ($[cc(bb), {}^3S_1\text{-}\bar{\mathbf{3}}]$ and $[cc(bb), {}^1S_0\text{-}\mathbf{6}]$) and four bc-diquark configurations ($[bc, {}^3S_1\text{-}\bar{\mathbf{3}}]$, $[bc, {}^3S_1\text{-}\mathbf{6}]$, $[bc, {}^1S_0\text{-}\bar{\mathbf{3}}]$, and $[bc, {}^1S_0\text{-}\mathbf{6}]$) are considered in the calculation. Numerical results indicate that the $[cc, {}^3S_1\text{-}\bar{\mathbf{3}}]$ diquark provides dominant contribution for Ξ_{cc} (T_{cc}) production, and a considerable number of Ξ_{cc} (T_{cc}) can be produced. Because the event topologies for ultraperipheral collision are very clear, the background from various QCD interactions can be suppressed, hence the experimental investigation for Ξ_{cc} and T_{cc} is feasible. The productions for $\Xi_{bc/bb}$ are also discussed, leaving only a slight possibility for Ξ_{bc} through photon-gluon fusion with ultraperipheral collisions at the FCC.

I. INTRODUCTION

The existence of doubly heavy baryons, predicted by the quark model, has been a mystery for more than a half century until the LHCb Collaboration observed the Ξ_{cc}^{++} signal via $\Lambda_c^+ K^- \pi^+ \pi^+$ channel [1] and further confirmed via $\Xi_{cc}^{++} \to \Xi_c^+ \pi^+$ [2,3]. And recently, doubly heavy tetraquark $T_{cc}^+(3875)$ has also been seen through $T_{cc}^+(3875) \to D^0 D^0 \pi^+$ at the LHCb [4]. The doubly heavy component within those hadrons indicates a typically nonrelativistic feature, hence they tend to stay close and form heavy-heavy diquarks. In this way, the production of doubly heavy hadrons can be described by the nonrelativistic QCD (NRQCD) [5], which factorizes the production into two steps. The first step is to produce heavy-heavy diquarks with given spin-color structure, e.g., $[cc, {}^3S_1\text{-}\bar{\mathbf{3}})]$, $[cc, {}^1S_0\text{-}\mathbf{6}]$, which is perturbatively calculable. The second step is reserved for the hadronization of the diquark though unperturbative QCD mechanism, e.g.,

fragmentation, which is encoded into long-distance matrix elements (LDMEs) and fragmentation function.

Among the earlier theoretical investigations toward the production of doubly heavy baryons, only the color antitriplet diquark configuration is proposed [6–12]. As indicated in Ref. [13], the contribution from color sextuplet holds the same level with the color antitriplet at the framework of NRQCD factorization. In this way, there are extensive studies for the production channels of $\Xi_{QQ'}$ through $e^+ e^-$ [14,15], $\gamma\gamma$ [16,17], ep [18,19], and pp [20,21] collisions, and also the indirect productions through W, Z, Higgs, and top quark [22–25]. Based on the diquark-diquark picture, the productions for exotic tetraquark T_{cc} are also investigated [26–28]. The above studies may provide opportunities to experimental researches for doubly heavy hadrons and make a new test window for NRQCD factorization formalism at various colliders.

The ultraperipheral heavy ion collisions (UPCs) [29–33] are ideal to study double heavy hadrons due to their low event multiplicity and efficient signal selection, and the dissociation effect caused by thermal medium can be avoided [34]. The equivalent real photon interaction can be studied if the ion impact parameter is much larger than the ion radius,[1] in which the elastic scattering is a pure QED process. The unbroken ion will cause less additional

---

*Corresponding author: jiangjun87@sdu.edu.cn
†Corresponding author: bingwei@scu.edu.cn
‡yanghao2023@scu.edu.cn

[1]The term "ultraperipheral" means collisions with distance $b > R_1 + R_2$ and should be distinguished from "peripheral" collision where $b \approx R_1 + R_2$.

calorimetric signals and large signal rapidity gap with the produced state, hence lead to efficient signal selection. Further more, the photon density is proportional to the square of ion charge Z under the equivalent photon approximation, e.g., the $\gamma - \gamma$ luminosity is enhanced by 82^4 in Pb-Pb collisions compared with electron bremsstrahlung [16,17], and the production cross sections via photon-photon and photon-gluon collisions for doubly heavy hadrons will be considerable. Therefore, we will explore the doubly heavy baryon and tetraquark production through elastic photon-photon and photon-gluon fusions at the LHC.

The rest of this paper is organized as follows. In Sec. II, we present the primary formulas employed in the calculation. In Sec. III, the numerical results and discussions toward doubly heavy baryon and tetraquark production are performed. The last section is reserved for summary and conclusions.

II. FORMULATION

The electromagnetic filed of high energy ions can be approximately identified to quasireal photon distribution where the longitudinal part is highly suppressed. Analogous to the von Weizsacker–Williams method [35,36], the equivalent photon energy spectrum can be formulated by [37]

$$n_{\gamma/A}(\omega) = \frac{2Z^2\alpha}{\pi}\left[\xi K_0(\xi)K_1(\xi) - \frac{\xi^2}{2}(K_1(\xi)^2 - K_0^2(\xi))\right], \quad (1)$$

where ω is photon energy, Z is ion charge, α is the electromagnetic fine structure constant, $\xi = \omega R/\gamma_L\beta$, R is the ionic radius, γ_L, β are Lorentz factors, and $K_{0/1}(\xi)$ are the modified Bessel functions.

In this paper, we will refer to elastic photoproduction (photon-photon) cross section for one (two) photon process $A + B \to A + X$ ($A + B \to A + X + B$). The event topologies for those processes are very clean: very forward ions measured far from the collision point and a few centrally

produced particles; the photon momenta can be precisely measured, allowing one to reconstruct any missing degrees of freedom in the final state; the background from parton-parton interaction can be sufficiently suppressed if no strong interaction is involved.

The total cross section for elastic photoproduction of $A + B \to A + X$ can be factorized as

$$\sigma(A + B \to A + X)$$
$$= \int \frac{d\omega}{\omega}n_{\gamma/A}(\omega)\int dx f_{g/B}(x)\hat{\sigma}(\gamma g \to X), \quad (2)$$

where $f_{g/B}(x)$ is the distribution function of gluon for nucleus B. For the elastic photon-photon collision, the total cross section of $A + B \to A + X + B$ is factorized into convolution of photon-photon luminosity and $\gamma\gamma \to X$ cross section,

$$\sigma(A + B \to A + X + B)$$
$$= \int \frac{d\omega_1}{\omega_1}n_1(\omega_1)\int \frac{d\omega_2}{\omega_2}n_2(\omega_2)\hat{\sigma}_{\gamma\gamma\to X}(W_{\gamma\gamma})$$
$$= \int dW_{\gamma\gamma}\int dY \frac{dL_{\gamma\gamma}}{dW_{\gamma\gamma}dY}\hat{\sigma}_{\gamma\gamma\to X}(W_{\gamma\gamma}). \quad (3)$$

Here $\frac{dL_{\gamma\gamma}}{dW_{\gamma\gamma}dY}$ is the equivalent photon luminosity,

$$\frac{dL_{\gamma\gamma}}{dW_{\gamma\gamma}dY} = \frac{2}{W_{\gamma\gamma}}n_1\left(\frac{W_{\gamma\gamma}}{2}\exp^Y\right)n_2\left(\frac{W_{\gamma\gamma}}{2}\exp^{-Y}\right), \quad (4)$$

Y is the rapidity of the $\gamma - \gamma$ system with $Y = \frac{1}{2}\ln\frac{\omega_1}{\omega_2}$. The effective photon-photon luminosities dL_γ/dW_γ (with Y integrated) for various ion-ion collisions are given in Fig. 1. Throughout our description, the survival probabilities, which correspond to the probability of scattered ions not to dissociate due to the secondary soft interactions, are set to be 100%. Detailed calculation of the survival factors may
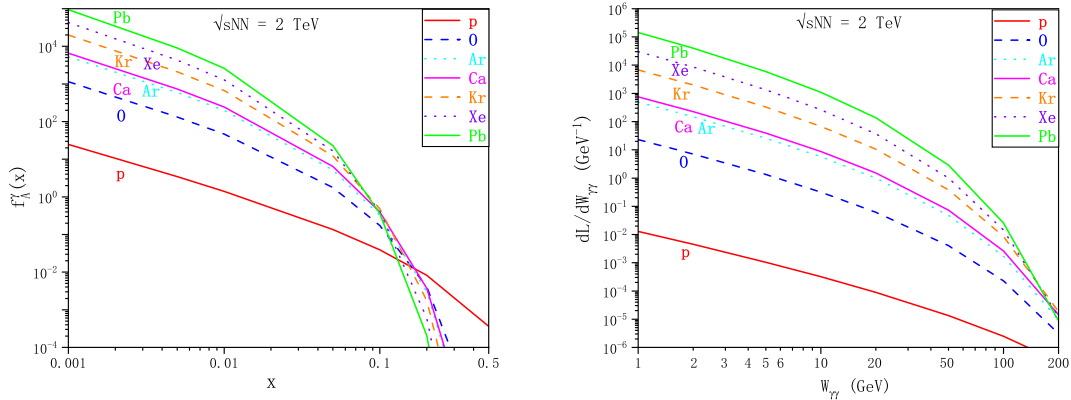

FIG. 1. Functions of ultraperipheral photon spectra $f_A^\gamma(x) = n(\omega)/x$ and comparison of the effective photon-photon luminosities $dL_{\gamma\gamma}/dW_{\gamma\gamma}$ for various ultraperipheral ion collisions with $\sqrt{s_{NN}} = 2$ TeV.
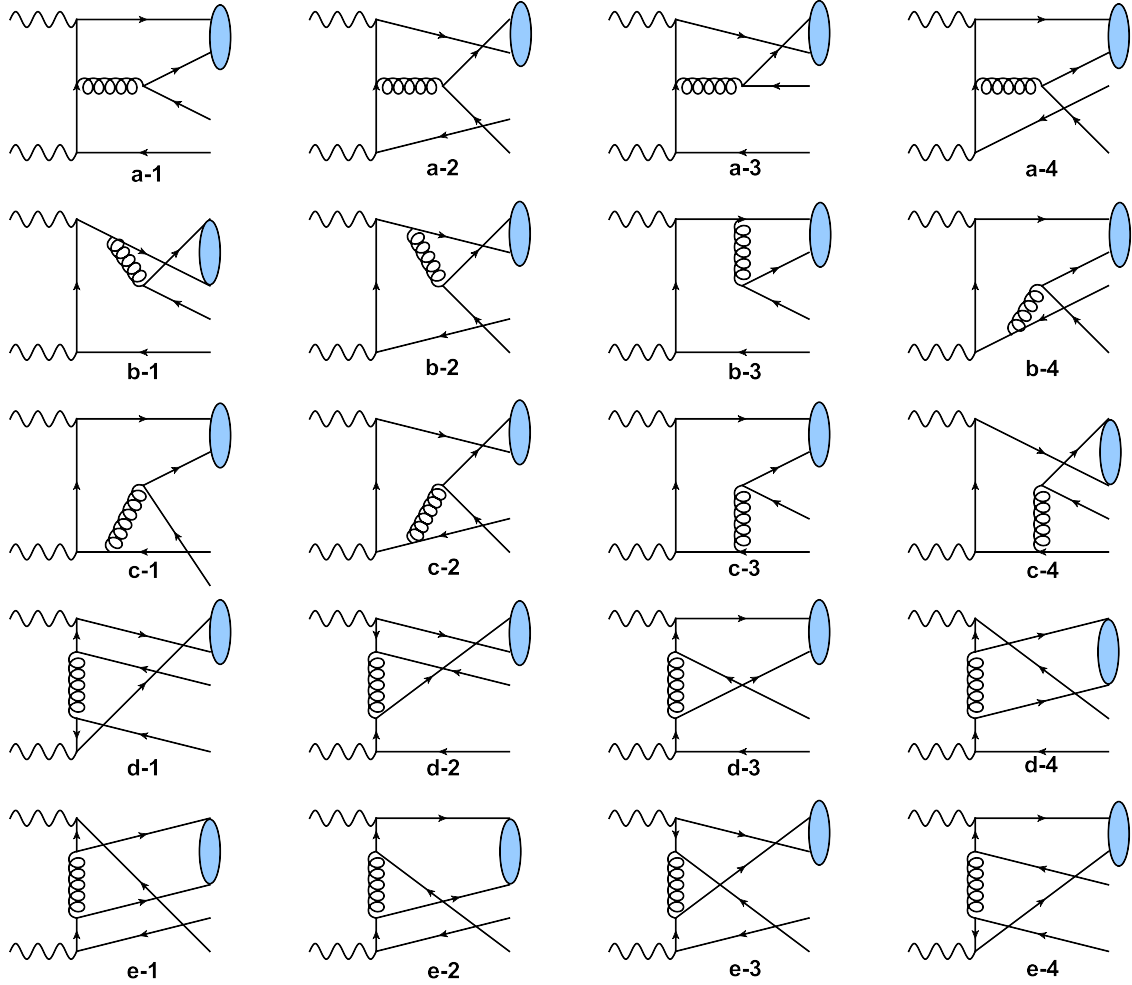
FIG. 2. Half Feynman diagrams for $\gamma\gamma \to (QQ)[n] + \bar{Q}\bar{Q}$, where Q represents the heavy charm or bottom quark, $[n]$ is the spin-color number for the QQ-diquark. The remaining diagrams can be obtained via exchanging initial two photons. The topologies, e.g., a-3, will not exist for $QQ'[n]$ production, leaving only 20 Feynman diagrams in total.

depend on the impact parameter space for each ions. We neglect this probability in the following analysis, the effect is estimated to be less than 20% as indicated in Ref. [38].

For the elastic photon-photon fusion, there are 40 Feynman diagrams in total for $\gamma\gamma \to (QQ)[n] + \bar{Q} + \bar{Q}$ at leading order (LO),[2] half of them are given in Fig. 2, another 20 diagrams can be obtained via exchanging initial photons. The topologies labeled b-(1,2,3) are fragmentation diagrams with one of the final heavy quark fragmenting into the (QQ) diquark. According to NRQCD factorization formalism, the cross section for $\gamma\gamma \to (QQ')[n] + \bar{Q} + \overline{Q'}$ takes the form

$$\hat{\sigma}_{\gamma\gamma \to H_{QQ'} + \bar{Q} + \overline{Q'}} = \sum_n \hat{\sigma}(\gamma\gamma \to (QQ')[n] + \bar{Q} + \overline{Q'})\langle \mathcal{O}^H(n)\rangle,$$

(5)

---

[2]We note that there are only 20 Feynman diagrams for Ξ_{bc} production.

where $\langle \mathrm{O}^H(n)\rangle$ is the LDME for $(QQ')[n]$, which represents the inclusive transition probability of the $(QQ')[n]$ diquark state into doubly heavy $\Xi_{QQ'}/T_{QQ'}$ hadrons, and $[n]$ stands for the spin-color numbers of $(QQ')[n]$ diquark state.

The short-distance cross section for $\gamma\gamma \to (QQ')[n] + \bar{Q} + \overline{Q'}$,

$$d\hat{\sigma}(\gamma\gamma \to (QQ')[n] + \bar{Q} + \overline{Q'})$$
$$= \frac{1}{2}\frac{1}{2}\frac{1}{2s_{\gamma\gamma}}\overline{\sum}|\mathcal{M}(\gamma\gamma \to (QQ')[n] + \bar{Q} + \overline{Q'})|^2 dPS_3,$$ (6)

can be obtained after integrating the phase space. Here the two $\frac{1}{2}$ factors are the polarization average for initial photons, $\frac{1}{2s_{\gamma\gamma}}$ is the photon-photon flux, and an extra $\frac{1}{2}$ factor is needed if $Q = Q'$ due to identical particles average.

In the elastic photoproduction of Ξ_{cc}, apart from similar topologies (one photon is replaced by a gluon) in Fig. 2, more topologies are involved, see Fig. 3. An extra $1/8$ color factor is needed in Eq. (6).
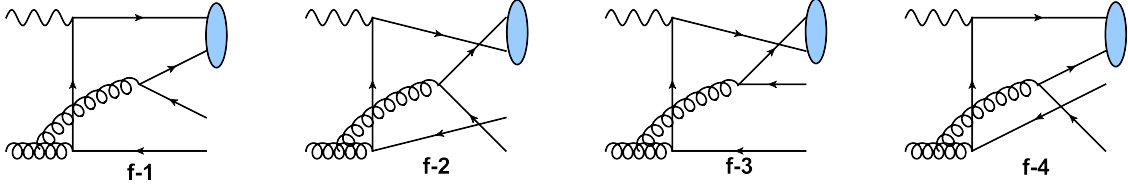
FIG. 3. Extra Feynman diagrams for $\gamma g \to (QQ)[n] + \bar{Q}\bar{Q}$, where Q represents the heavy charm or bottom quark, $[n]$ is the spin-color number for the QQ-diquark. The remaining diagrams can be obtained via exchanging initial photon and gluon.

The hard scattering amplitude $\mathcal{M}$ for $\gamma\gamma(\gamma g) \to (QQ')[n] + \bar{Q} + \overline{Q'}$ can be formulated as

$$
\begin{aligned}
\mathcal{M}((QQ')[n]) &= \epsilon^\alpha \epsilon^\beta \bar{u}(p_Q, \sigma_1) \gamma_{\alpha_n} s_f(q_{n-1}, m_Q) \cdots s_f(q_1, m_Q) \gamma_{\alpha_1} v(p_{\bar{Q}}, \sigma_4) \\
&\times \bar{u}(p_{Q'}, \sigma_2) \gamma'_{\beta_1} s_f(q'_1, m_{Q'}) \cdots s_f(q'_{m-1}, m_{Q'}) \gamma'_{\beta_m} v(p_{\overline{Q'}}, \sigma_3) \\
&\times \mathcal{B}(S, \sigma_1, \sigma_2; p_{QQ'}, M_{QQ'}) \times \mathcal{C} \times \mathcal{G}.
\end{aligned} \tag{7}
$$

Here, $\epsilon^{\alpha/\beta}$ are the polarization vectors for initial states, σ_i stands for the spin state of the final heavy quark, and $s_f(q, m)$ is the fermion propagator between two interaction vertices. $\mathcal{B}(S, \sigma_1, \sigma_2; p_{QQ'}, M_{QQ'})$ represents the wave function of heavy diquark $(QQ')[n]$, $\mathcal{C}$ is the SU(3) color factor, and $\mathcal{G}$ is the gluon propagator.

In computing the heavy quarkonium production cross sections, the covariant spin-projector method is applied to identify spin-singlet and spin-triplet amplitudes. At the leading order of relative velocity expansion of NRQCD, the standard spin projector [39] can be written as

$$
v(p_{\bar{Q}})\bar{u}(p_{Q'}) = \frac{1}{2\sqrt{m_{QQ'}}}\not\epsilon(p_{QQ'})(\not p_{QQ'} + m_{QQ'}), \tag{8}
$$

where $\epsilon(p_{QQ'})$ is the polarization vector for the spin-triplet state and the projector for the spin-singlet state can be obtained by replacing the $\not\epsilon(p_{QQ'})$ with γ^5.

To project the amplitude in Eq. (7) into a given spin state, we need translate the fermion chain

$$
a = \bar{u}(p_Q, \sigma_1)\gamma_{\alpha_n} s_f(q_{n-1}, m_Q) \cdots s_f(q_1, m_Q)\gamma_{\alpha_1} v(p_{\bar{Q}}, \sigma_4) \tag{9}
$$

into

$$
\begin{aligned}
a = a^T &= v^T(p_{\bar{Q}}, \sigma_4)\gamma^T_{\alpha_1} s^T_f(q_1, m_Q) \cdots s^T_f(q_{n-1}, m_Q)\gamma^T_{\alpha_n}\bar{u}^T(p_Q, \sigma_1) \\
&= v^T(p_{\bar{Q}}, \sigma_4)\mathcal{CC}^{-1}\gamma^T_{\alpha_1}\mathcal{CC}^{-1} s^T_f(q_1, m_Q)\mathcal{CC}^{-1} \cdots \mathcal{CC}^{-1} s^T_f(q_{n-1}, m_Q)\mathcal{CC}^{-1}\gamma^T_{\alpha_n}\mathcal{CC}^{-1}\bar{u}^T(p_Q, \sigma_1) \\
&= (-1)^{n+1}\bar{u}(p_{\bar{Q}}, \sigma_4)\gamma_{\alpha_1} s_f(-q_1, m_Q) \cdots s_f(-q_{n-1}, m_Q)\gamma_{\alpha_n} v(p_Q, \sigma_1)
\end{aligned} \tag{10}
$$

with the help of charge conjugation operator $\mathcal{C} = -i\gamma^2\gamma^0$ and the relations

$$
\begin{gathered}
\mathcal{CC}^{-1} = 1, \qquad \mathcal{C}^{-1}\gamma^T_{\alpha_i}\mathcal{C} = -\gamma_{\alpha_i}, \qquad \mathcal{C}^{-1} s^T_f(q_i, m_Q)\mathcal{C} = s_f(-q_i, m_Q), \\
v^T(p_{\bar{Q}}, \sigma_4)\mathcal{C} = -\bar{u}(p_{\bar{Q}}, \sigma_4), \qquad \mathcal{C}^{-1}\bar{u}^T(p_Q, \sigma_1) = v(p_Q, \sigma_1).
\end{gathered} \tag{11}
$$

TABLE I. The nucleon-nucleon (NN) c.m. energy $\sqrt{s_{NN}}$, effective charge radius R_A [53], and integrated luminosity per typical run $\mathcal{L}_{int}$ for ultraperipheral collisions at HL-LHC and FCC.

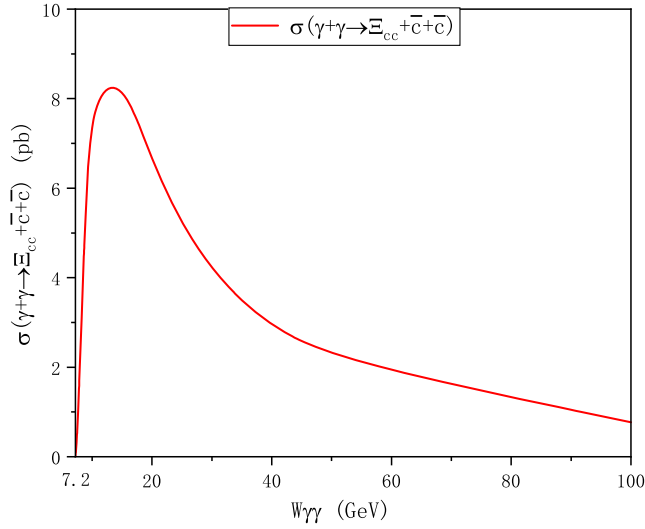| System	Pb-Pb	Xe-Xe	Kr-Kr	Ar-Ar	Ca-Ca	O-O	p-Pb	p-p	Pb-Pb	p-Pb	p-p
$\sqrt{s_{NN}}$ (TeV)	5.52	5.86	6.46	6.3	7.0	7.0	8.8	14	39.4	62.8	100
R_A (fm)	7.1	6.1	5.1	4.1	4.1	3.1	0.7, 7.1	0.7	7.1	0.7, 7.1	0.7
$\mathcal{L}_{int}$	5 nb^{-1}	30 nb^{-1}	120 nb^{-1}	1.1 pb^{-1}	0.8 pb^{-1}	12 pb^{-1}	1 pb^{-1}	150 fb^{-1}	110 nb^{-1}	29 pb^{-1}	1 ab^{-1}

FIG. 4. The cross section for $\gamma + \gamma \rightarrow \Xi_{cc}[^3S_1\text{-}\bar{\mathbf{3}} + {}^1S_0\text{-}\mathbf{6}] + \bar{c}\bar{c}$ versus c.m. energy ($W_{\gamma\gamma}$) of photon-photon fusion.

According to SU(3) decomposition: $\mathbf{3} \otimes \mathbf{3} = \bar{\mathbf{3}} \oplus \mathbf{6}$, the heavy diquark could be either color antitriplet $\bar{\mathbf{3}}$ which is attractive in, e.g., one-gluon exchange potential [40,41], or color sextuplet $\mathbf{6}$ which is repulsive. The color factor $\mathcal{C}$ in Eq. (7) is defined as

$$\mathcal{C} = \mathcal{C}_{ijk} = \mathcal{N}_c \times \sum_{m,n}(T^a)_{im}(T^a)_{jn} \times G_{mnk}, \quad (12)$$

where $\mathcal{N}_c = \frac{1}{\sqrt{2}}$ is the normalization factor, the factor G_{mnk} stands for the (anti)symmetric tensor (ϵ_{mnk}) f_{mnk} for the color (antitriplet $\bar{\mathbf{3}}$) sextuplet $\mathbf{6}$, which satisfies the following relations:

$$\epsilon_{mnk}\epsilon_{m'n'k} = \delta_{mm'}\delta_{nn'} - \delta_{mn'}\delta_{nm'},$$
$$f_{mnk}f_{m'n'k} = \delta_{mm'}\delta_{nn'} + \delta_{mn'}\delta_{nm'}. \quad (13)$$

In the calculation, the *Mathematica* package FEYNARTS [42] is used to generate Feynman diagrams; FEYNCALC [43]

and FEYNCALCFORMLINK [44] are used to handle the algebraic calculation; the overall phase-space integrals are performed numerically by using the package CUBA [45].

III. NUMERICAL RESULTS AND DISCUSSIONS

The LDME for antitriplet $h_{\bar{\mathbf{3}}}$ can be related to the matrix element $|\langle 0|\chi^+\boldsymbol{\sigma}\psi|^3S_1\rangle|^2$, which is the transition of a $Q\overline{Q}'$ pair into a $^3S_1$ quarkonium, by assuming that the potentials for binding $Q\overline{Q}'$ and QQ' states are all hydrogenlike. In this way, the radial wave function at the origin $R_{QQ'}(0)$ is related to $h_{\bar{\mathbf{3}}}$ by

$$h_{\bar{\mathbf{3}}} = |\Psi_{QQ'}(0)|^2 = \frac{1}{4\pi}|R_{QQ'}(0)|^2. \quad (14)$$

Note that the LDME $h_{\bar{\mathbf{3}}}$ does not consider the dissociation effect of the diquark, which could be small in the absence of quark gluon plasma (QGP), but would decrease the hadronization probability of the diquark; our present estimations can be treated as an upper limit for the production channels. According to the velocity scaling rule of NRQCD [5], the LDME for color sextuplet $h_{\mathbf{6}}$ is on same order of $h_{\bar{\mathbf{3}}}$, hence we take $h_{\mathbf{6}} = h_{\bar{\mathbf{3}}}$ in our calculation. The input parameters are taken as

$$\alpha = 1/137.065, \qquad m_p = 0.9315 \text{ GeV},$$
$$m_c = 1.8 \text{ GeV}, \qquad m_b = 5.1 \text{ GeV}$$
$$|\Psi_{cc}(0)|^2 = 0.039 \text{ GeV}^3, \qquad |\Psi_{bc}(0)|^2 = 0.065 \text{ GeV}^3,$$
$$|\Psi_{bb}(0)|^2 = 0.152 \text{ GeV}^3, \quad (15)$$

where the wave functions at the origin are taken from Refs. [7,46] with above heavy quark masses.

The one-loop formula $\frac{\alpha_s(\mu)}{4\pi} = \frac{1}{\beta_0 L}$ for the running coupling constant is adopted in our calculation, where $L = \ln(\mu^2/\Lambda_{\text{QCD}})^2$, $\beta_0 = \frac{11}{3}C_A - \frac{4}{3}T_F n_f$ with $n_f = 4$, $\Lambda_{\text{QCD}} = 297$ MeV for Ξ_{cc} production, and $n_f = 5$, $\Lambda_{\text{QCD}} = 214$ MeV for $\Xi_{bc(bb)}$ production. The renormalization scale

TABLE II. The cross sections for $\gamma + \gamma \rightarrow \Xi_{cc}[cc, n] + \bar{c}\bar{c}$ through UPCs at the HL-LHC and FCC.

| Collisions	$\sqrt{s_{NN}}$ (TeV)	$\Xi_{cc}[cc, {}^3S_1\text{-}\bar{\mathbf{3}}]$	$\Xi_{cc}[cc, {}^1S_0\text{-}\mathbf{6}]$	Total	$N_{\Xi_{cc}}$
Pb-Pb	5.52	270 nb	9.53 nb	279.5 nb	1.40×10^3
Xe-Xe	5.86	65.9 nb	2.38 nb	68.28 nb	2.05×10^3
Kr-Kr	6.46	17.8 nb	0.663 nb	18.46 nb	2.21×10^3
Ar-Ar	6.3	1.36 nb	0.0518 nb	1.411 nb	1.55×10^3
Ca-Ca	7.0	2.31 nb	0.0886 nb	2.398 nb	1.92×10^3
O-O	7.0	77.1 pb	3.03 pb	80.13 pb	9.61×10^2
p-Pb	8.8	203 pb	8.33 pb	211.33 pb	2.11×10^2
p-p	14	89.6 fb	3.99 fb	93.59 fb	1.43×10^4
Pb-Pb	39.4	1780 nb	74.5 nb	1854 nb	2.04×10^5
p-Pb	62.8	728 pb	32.8 pb	760.8 pb	2.20×10^4
p-p	100	233 fb	10.9 fb	243.9 fb	2.44×10^5
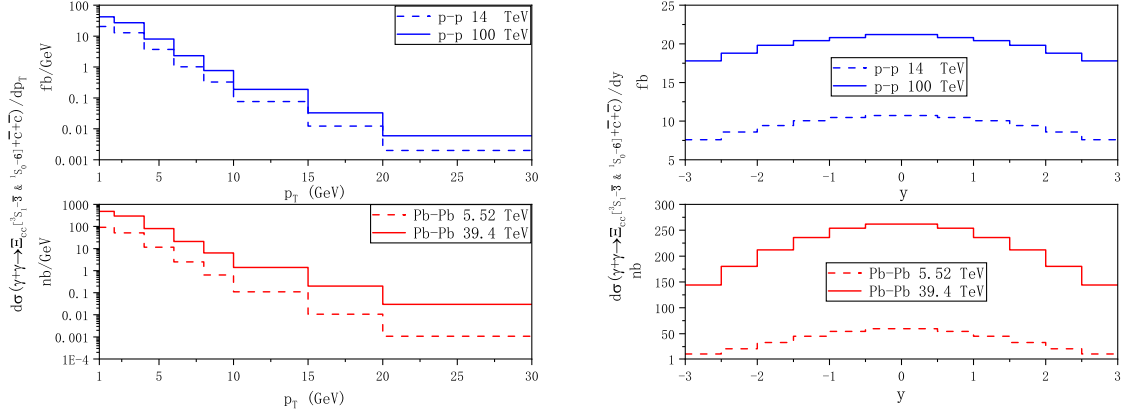
FIG. 5. The transverse momentum p_T and rapidity y distributions for Ξ_{cc} production via ultraperipheral collisions. Here, for the p_T distribution, y is cut to be $[-3, 3]$; for the y distribution, p_T is cut to be 1–30 GeV.

is set to be transverse mass of $\Xi_{QQ'}$ with $\mu_r = \sqrt{m_{\Xi_{QQ'}}^2 + p_t^2}$. The Les Houches Accord parton distribution function [47] is adopted for the gluon parton distribution functions in ions with datasets labeled "nCTEQ15WZ" [48] and the factorization scale μ_f is set to be the same as renormalization scale.

A. Elastic photon-photon production

The interaction of heavy ions at large impact parameters is purely electromagnetical; such an interaction can be considered as real photon-photon fusion. The generic characteristics of photon-photon fusion in ultraperipheral ion-ion collisions at HL-LHC [49,50] and Future Circular Collider (FCC) [51,52] energies are collected in Table I. Compared to the e^+e^- and p-p collisions, the typical features of photon-photon collision via UPCs are the lack of pileup and highly photon flux boost (Z^4). Hence, the event signatures will be clear and the reconstruction efficiency can be improved.

The photon-photon cross section for Ξ_{cc} versus $W_{\gamma\gamma}$ within default parameters is given in Fig. 4, and the contributions from color antitriplet $\bar{\mathbf{3}}$ and sextuplet $\mathbf{6}$ are collected. The cross section reaches its maximal value just several GeV above the threshold and decreases with c.m. energy of photon-photon system. As the effective photon-photon luminosities decrease dramatically with $W_{\gamma\gamma}$, the main contribution can be only related to small $W_{\gamma\gamma}$ values, typically from $4m_c$ to 50 GeV. The cross sections for each spin-color state of Ξ_{cc} are listed in Table II. The contribution from $cc[^1S_0\text{-}\mathbf{6}]$ is only $3\% \sim 5\%$ to that of $cc[^3S_1\text{-}\bar{\mathbf{3}}]$, the ratio holds also for Ξ_{bb}.

Supposing the integrated luminosities in Table I and aggregating the contributions for diquark in all spin-color structures, the produced Ξ_{cc} numbers via various UPCs at the HL-LHC are around 10^3. As the collision energies and luminosities are highly improved at the FCC, the yields for Ξ_{cc} can be increased by one or two magnitudes, reaching

2.44×10^5 for p-p in 100 TeV with a integrated luminosity of 1 ab^{-1}. To estimate the event, we set the relative possibilities for various light quarks as $u:d:s \sim 1:1:0.3$, and the reconstruction channel $\mathrm{Br}(\Xi_{cc}^{++} \to \Lambda_c^+ K^- \pi^+ \pi^+) \approx 10\%$ [54], $\mathrm{Br}(\Lambda_c^+ \to pK^-\pi^+) \approx 5\%$ [55]. Considering some detection efficiencies, Ξ_{cc}^{++} events via ultraperipheral collisions may be expected at the FCC.

As the number of events corresponding to $\gamma + \gamma \to \Xi_{cc}[cc, {}^3S_1\text{-}\bar{\mathbf{3}} + {}^1S_0\text{-}\mathbf{6}] + \bar{c}\,\bar{c}$ is considerable, it is worthy to perform a more elaborate phenomenological analysis. The transverse momentum and rapidity distributions of Ξ_{cc} through UPCs are given in Fig. 5, with the $p_T = 1$–30 GeV and $y = [-3, 3]$. The cross sections decease rapidly versus high p_T, showing a logarithmic dependence of p_T. As the UPCs are characterized by a large rapidity gap between the produced state and the interacting nucleus accompanied by forward neutron emission from the deexcitation of the nucleus [31], the resulting rapidity distribution is relatively narrow and centered at midrapidity. For the equal energy beam collisions, the rapidity distributions show a symmetric behavior. To estimate the theoretical uncertainties caused by charm mass and renormalization scale, we set the charm mass to be 1.7, 1.8, and 1.9 GeV, and the renormalization scales are chosen to be $\frac{1}{2}$, 1, and 2 times of Ξ_{cc} transverse mass, see Table III.

We also study the production cross sections for $\Xi_{bc/bb}$ via various UPCs at HL-LHC and FCC; the numerical

TABLE III. The cross sections for $\Xi_{cc}[cc, {}^3S_1\text{-}\bar{\mathbf{3}}]$ ($\Xi_{cc}[cc, {}^1S_0\text{-}\mathbf{6}]$) (in unit of nanobarn) under different m_c and renormalization scales through ultraperipheral Pb-Pb collision at 5.52 TeV.

	m_c (GeV)		
μ	1.7	1.8	1.9
$\frac{1}{2}\sqrt{4m_c^2 + p_T^2}$	752 (25.8)	496 (16.9)	334 (11.4)
$\sqrt{4m_c^2 + p_T^2}$	404 (14.3)	271 (9.53)	185 (6.48)
$2\sqrt{4m_c^2 + p_T^2}$	252 (9.09)	170 (6.10)	117 (4.18)

results for each spin-color states are listed in Tables IV and V. As the heavy constituent for bc quark is different, the exchange asymmetry for identical particles does not hold; hence all diquark structures for spin-color states in $bc[^3S_1\text{-}\bar{\mathbf{3}}]$, $bc[^3S_1\text{-}\mathbf{6}]$, $bc[^1S_0\text{-}\bar{\mathbf{3}}]$, and $bc[^1S_0\text{-}\mathbf{6}]$ will contribute in a comparable level with slight suppression for the spin singlet, as indicated by previous predictions [10,11]. Furthermore, the cross section for color antitriplet $\bar{\mathbf{3}}$ is 2

TABLE IV. The cross sections for $\gamma + \gamma \to \Xi_{bc}[bc, n] + \bar{b}\bar{c}$ through UPCs at the HL-LHC and FCC.

Collisions	$\sqrt{s_{NN}}$ (TeV)	$\Xi_{bc}[bc, {}^3S_1\text{-}\bar{\mathbf{3}}]$	$\Xi_{bc}[bc, {}^3S_1\text{-}\mathbf{6}]$	$\Xi_{bc}[bc, {}^1S_0\text{-}\bar{\mathbf{3}}]$	$\Xi_{bc}[bc, {}^1S_0\text{-}\mathbf{6}]$	Total
Pb-Pb	5.52	850 pb	425 pb	335 pb	167.5 pb	1777 pb
Xe-Xe	5.86	221 pb	110 pb	88 pb	44 pb	463 pb
Kr-Kr	6.46	64.3 pb	32.1 pb	25.8 pb	12.9 pb	135.1 pb
Ar-Ar	6.3	5.16 pb	2.58 pb	2.08 pb	1.04 pb	10.86 pb
Ca-Ca	7.0	8.94 pb	4.47 pb	3.62 pb	1.81 pb	18.84 pb
O-O	7.0	315 fb	157 fb	128 fb	64 fb	664 fb
p-Pb	8.8	910 fb	455 fb	374 fb	187 fb	1926 fb
p-p	14	0.472 fb	0.236 fb	0.197 fb	0.098 fb	1.003 fb
Pb-Pb	39.4	8.32 nb	4.16 nb	3.44 nb	1.72 nb	17.64 nb
p-Pb	62.8	3.92 pb	1.96 pb	1.65 pb	0.825 pb	8.355 pb
p-p	100	1.36 fb	0.68 fb	0.58 fb	0.29 fb	2.91 fb

TABLE V. The cross sections for $\gamma + \gamma \to \Xi_{bb}[bb, n] + \bar{b}\bar{b}$ through UPCs at the LHC and FCC.

Collisions	$\sqrt{s_{NN}}$ (TeV)	$\sigma(\gamma\gamma \to \Xi_{bb}[bb, {}^3S_1\text{-}\bar{\mathbf{3}}] + \bar{b}\bar{b})$	$\sigma(\gamma\gamma \to \Xi_{bb}[bb, {}^1S_0\text{-}\mathbf{6}] + \bar{b}\bar{b})$	Total
Pb-Pb	5.52	37.0 pb	1.12 pb	38.12 pb
Xe-Xe	5.86	10.2 pb	0.323 pb	10.52 pb
Kr-Kr	6.46	3.18 pb	0.105 pb	3.285 pb
Ar-Ar	6.3	265 fb	9.09 fb	274.1 fb
Ca-Ca	7.0	470 fb	16.3 fb	486.3 fb
O-O	7.0	17.4 fb	0.629 fb	18.02 fb
p-Pb	8.8	54.1 fb	2.08 fb	56.18 fb
p-p	14	32 ab	1.4 ab	33.4 ab
Pb-Pb	39.4	514 pb	20.4 pb	534.4 nb
p-Pb	62.8	273 fb	12 fb	285 fb
p-p	100	101 ab	4.74 ab	105.7 ab

TABLE VI. The cross sections for $g + \gamma \to \Xi_{cc}[cc, n] + \bar{c}\bar{c}$ through elastic photoproduction at the HL-LHC and FCC. The cross sections in brackets are the contributions from $\gamma + g$ channel, which are different from $g + \gamma$ channel in the p-Pb collision; while the two contributions are absolutely equal for same ions collision, e.g., Pb-Pb. The total cross sections contain all the $g + \gamma$ and $\gamma + g$ channels.

| Collisions	$\sqrt{s_{NN}}$ (TeV)	$\Xi_{cc}[cc, {}^3S_1\text{-}\bar{\mathbf{3}}]$	$\Xi_{cc}[cc, {}^1S_0\text{-}\mathbf{6}]$	Total	$N_{\Xi_{cc}}$
Pb-Pb	5.52	82.9 μb	7.09 μb	179.98 μb	9.00×10^5
Xe-Xe	5.86	24.9 μb	2.14 μb	54.08 μb	1.62×10^6
Kr-Kr	6.46	8.34 μb	0.72 μb	18.12 μb	2.17×10^6
Ar-Ar	6.3	1.08 μb	0.094 μb	2.35 μb	2.58×10^6
Ca-Ca	7.0	1.46 μb	0.127 μb	3.17 μb	2.53×10^6
O-O	7.0	108 nb	9.44 nb	234.88 nb	2.81×10^6
p-Pb	8.8	628 (44.2) nb	54.2 (4.01) nb	730.41 nb	7.30×10^5
p-p	14	325 pb	29.6 pb	709.2 pb	1.06×10^8
Pb-Pb	39.4	374 μb	34.3 μb	816.6 μb	8.98×10^7
p-Pb	62.8	2.75(0.14) μb	0.25(0.013) μb	3.15 μb	9.13×10^7
p-p	100	1090 pb	103 pb	2386 pb	2.38×10^9
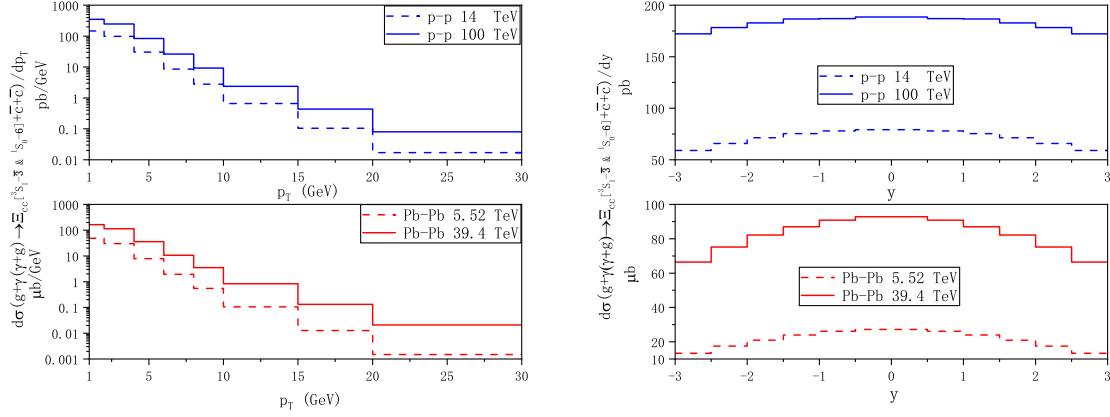
FIG. 6.   The transverse momentum p_T and rapidity y distributions for Ξ_{cc} production via semielastic ion-ion collisions. Here, for the p_T distribution, y is cut to be $[-3, 3]$; for the y distribution, p_T is cut to be 1–30 GeV.

times of sextuplet **6** in the same spin state ($^1S_0$ or $^3S_1$) due to SU(3) algebra. At the HL-LHC, only tens of Ξ_{bc} could be produced and in thousands for the FCC. For the Ξ_{bb}, the production cross sections are further suppressed. Hence, the phenomenological investigation for $\Xi_{bc/bb}$ through ultraperipheral ion-ion collisions may not be feasible.

B. Elastic photoproduction

In this subsection, we shall discuss the cross sections for the $\Xi_{cc(bc/bb)}$ production through elastic photoproduction $A + B \rightarrow A + \Xi_{cc(bc/bb)} + \bar{c}\bar{c}(\bar{b}\bar{c}/\bar{b}\bar{b}) + X$ at the LHC, and the productions for doubly heavy tetraquark are also discussed. Different from photoproduction in the electron-ion collision, where only the $\gamma + g$ channel will contribute with one photon produced by electron and one gluon produced by ion, the $g + \gamma$ channel also needs to be take into account. For the same ion collision, e.g., Pb-Pb, the two channels will lead to equal cross section; while for the p-Pb collision, the luminosity is enhanced by $1 \times Z^2$ (Z is charge number of Pb) for the $g + \gamma$ channel and only enhanced by $1 \times A$ (A is nucleus number of Pb) for the $\gamma + g$ channel, thus the contribution from $\gamma + g$ is negligible. In the following analysis, the contributions for both channels are given.

The elastic photoproduction cross sections for each spin-color state of Ξ_{cc} are listed in Table VI. Compared with elastic photon-photon production, the production ratios for $[cc, {}^1S_0\text{-}\mathbf{6}]/[cc, {}^3S_1\text{-}\bar{\mathbf{3}}]$ increase to $8\% \sim 9\%$. Supposing the integrated luminosities in Table I and collecting all the diquark structures, the produced Ξ_{cc} numbers via various elastic photoproduction at the HL-LHC and FCC are estimated in Table VI. In Pb-Pb collision with $\sqrt{s_{NN}} = 5.52$ TeV, the produced Ξ_{cc} is around 9×10^5 and increases to 10^8 for 14 TeV p-p collision due its high luminosity. To estimate the event, we adopt the reconstruction channel $\mathrm{Br}(\Xi_{cc}^{++} \rightarrow \Lambda_c^+ K^- \pi^+ \pi^+) \approx 10\%$ [54], $\mathrm{Br}(\Lambda_c^+ \rightarrow p K^+ \pi^+) \approx 5\%$ [55]. The event numbers

for Ξ_{cc}^{++} in this reconstruction channel are 1.95×10^3 for Pb-Pb collision and 2.3×10^5 for p-p collision. As the collision energies and luminosities are highly improved at the FCC, the yields for Ξ_{cc} can be increased by 1 or 2 magnitudes, leaving the possibility for further phenomenological investigation toward Ξ_{cc}. As the physical potential for observing doubly charmed baryons via the $g + \gamma(\gamma + g) \rightarrow \Xi_{cc}[cc, {}^3S_1\text{-}\bar{\mathbf{3}} + {}^1S_0\text{-}\mathbf{6}] + \bar{c}\bar{c}$ channel is large, we perform a detailed transverse momentum and rapidity distributions of Ξ_{cc} in Fig. 6, with the p_T cut to be 1–30 GeV and y set to be $[-3, 3]$.

Considering the number of produced $[cc]$ diquark is large, it is also possible to form a compact heavy-heavy tetraquark T_{cc} composed of cc diquark and light antidiquark (e.g., $\bar{u}\bar{d}$). The production mechanism of T_{cc} is similar to Ξ_{cc}: (i) the generation of $[cc, n]$ diquark at short distance; (ii) the subsequent formation of T_{cc} via combining two light quarks at long distance. The heavy-heavy diquark cluster in color antitriplet may served as heavy antiquark due to diquark-antiquark symmetry. Therefore, in the heavy quark limit, its fragmentation probability for combining light freedom to form doubly heavy tetraquarks can be approximately described as the probability to form heavy baryons from a heavy quark. The combining probability[3] is described by the fragmentation function $D_{\Lambda_c/c}(z)$ of charm quark to charm baryon at the heavy quark limit. The fragmentation fraction for $c \rightarrow \Lambda_c^+$ is measured to be 20.4% [56] at the LHC. In this way, the production cross sections for T_{cc}^+ can be estimated by $\frac{\sigma(T_{cc})}{\sigma(\Xi_{cc}) + \sigma(T_{cc})} = 20.4\%$, with $\sigma(T_{cc}) = \sigma(\Xi_{cc}) \times 25.6\%$, and yield total cross sections of 46 μb for Pb-Pb collision at 5.52 TeV and 181.5 pb for p-p collision at 14 TeV. Thus, the produced T_{cc}^+ numbers could be 2.3×10^5 and 2.72×10^7,

---

[3]In thermal medium, e.g., QGP, the cc diquark can be also dissociated by strong interaction with medium. Where in ultraperipheral collision, it is hard to form QGP. Hence, we only consider cc-diquark combination probability.

TABLE VII. The cross sections for $g + \gamma \rightarrow \Xi_{bc}[bc, n] + \bar{b}\bar{c}$ through elastic photoproduction at the HL-LHC and FCC. The cross sections in brackets are the contributions from the $\gamma + g$ channel, which are different from the $g + \gamma$ channel in the p-Pb collision; while the two contributions are absolutely equal for the same ion collisions. The total cross sections contain all the $g + \gamma$ and $\gamma + g$ channels.

Collisions	$\sqrt{s_{NN}}$ (TeV)	$\Xi_{bc}[bc,{}^3S_1\text{-}\bar{\mathbf{3}}]$	$\Xi_{bc}[bc,{}^3S_1\text{-}\mathbf{6}]$	$\Xi_{bc}[bc,{}^1S_0\text{-}\bar{\mathbf{3}}]$	$\Xi_{bc}[bc,{}^1S_0\text{-}\mathbf{6}]$	Total
Pb-Pb	5.52	619 nb	530 nb	184 nb	129 nb	2924 nb
Xe-Xe	5.86	193 nb	165 nb	57.9 nb	40.3 nb	912.4 nb
Kr-Kr	6.46	67.8 nb	57.8 nb	20.4 nb	14.1 nb	320.2 nb
Ar-Ar	6.3	8.88 nb	7.57 nb	2.67 nb	1.85 nb	41.94 nb
Ca-Ca	7.0	12.3 nb	10.5 nb	3.72 nb	2.57 nb	58.18 nb
O-O	7.0	932 pb	792 fb	281 pb	194 pb	4398 pb
p-Pb	8.8	5.07 (0.48) nb	4.32 (0.40) nb	1.52 (0.15) nb	1.06 (0.10) nb	13.1 nb
p-p	14	3.64 pb	3.06 pb	1.12 pb	0.76 pb	17.16 pb
Pb-Pb	39.4	4334 nb	3635 nb	1338 nb	907 nb	20.4 μb
p-Pb	62.8	32.5 (2.10) nb	27.2 (1.75) nb	10.0 (0.65) nb	6.81 (0.44) nb	81.45 nb
p-p	100	15.7 pb	13.0 pb	4.91 pb	3.29 pb	73.8 pb

TABLE VIII. The cross sections for $g + \gamma \rightarrow \Xi_{bb}[bb, n] + \bar{b}\bar{b}$ through elastic photoproduction at the HL-LHC and FCC. The cross sections in brackets are the contributions from $\gamma + g$ channel, which are different from $g + \gamma$ channel in the p-Pb collision; while the two contributions are absolutely equal for same ion collisions. The total cross sections contains all the $g + \gamma$ and $\gamma + g$ channels.

Collisions	$\sqrt{s_{NN}}$ (TeV)	$\sigma(g\gamma \rightarrow \Xi_{bb}[bb,{}^3S_1\text{-}\bar{\mathbf{3}}] + \bar{b}\bar{b})$	$\sigma(g\gamma \rightarrow \Xi_{bb}[bb,{}^1S_0\text{-}\mathbf{6}] + \bar{b}\bar{b})$	Total
Pb-Pb	5.52	60.0 nb	4.81 nb	129.62 nb
Xe-Xe	5.86	19.2 nb	1.56 nb	41.52 nb
Kr-Kr	6.46	6.96 nb	0.57 nb	15.06 nb
Ar-Ar	6.3	920 pb	75.6 pb	1991 pb
Ca-Ca	7.0	1299 pb	107 pb	2812 pb
O-O	7.0	99.5 pb	8.27 pb	215.5 pb
p-Pb	8.8	523 (58.8) pb	42.9 (5.11) pb	629.8 pb
p-p	14	454 fb	39.8 fb	987.6 fb
Pb-Pb	39.4	546 nb	48.1 nb	1188 nb
p-Pb	62.8	4.17 (0.30) nb	0.37 (0.027) nb	4.867 nb
p-p	100	2245 fb	206 fb	4902 fb

respectively. Considering T_{cc}^+ is reconstructed by the $D^0 D^0 \pi^+$ channel (supposed to be 100%), with subsequent D^0 decay $\mathrm{Br}(D^0 \rightarrow K^- \pi^+) = 3.94\%$ [57], the event number for T_{cc}^+ could be 357 and 4.2×10^4 via elastic photoproduction of Pb-Pb and p-p collisions. As for the FCC, the events could be further extended due to its better performance.

We also study the production cross sections for $\Xi_{bc/bb}$ via various elastic photoproduction at HL-LHC and FCC, and the numerical results for each spin-color states are listed in Tables VII and VIII. As the heavy constituents for bc quark are different, the exchange asymmetry for identical particles does not hold; hence all diquark structures for spin-color states in $bc[^3S_1\text{-}\bar{\mathbf{3}}]$, $bc[^3S_1\text{-}\mathbf{6}]$, $bc[^1S_0\text{-}\bar{\mathbf{3}}]$, and $bc[^1S_0\text{-}\mathbf{6}]$ will contribute in a comparable level. At the HL-LHC, 10^4–10^6 Ξ_{bc} could be produced, and increase to $2 \times 10^6 \sim 7 \times 10^7$ for FCC led to open possibility for phenomenological researches. For the Ξ_{bb}, the production

cross sections are further suppressed, only 648 Ξ_{bb} could be produced via Pb-Pb collision. Hence, the phenomenological investigation for Ξ_{bb} through ion-ion elastic photoproduction may be not feasible.

IV. SUMMARY AND CONCLUSIONS

In this work, we investigate the doubly heavy baryon and tetraquark production via photon-photon and photon-gluon fusion with various ultraperipheral ion-ion collisions in the framework of NRQCD factorization formalism. Two $cc(bb)$-diquark configurations, $[cc(bb), {}^3S_1\text{-}\bar{\mathbf{3}}]$ and $[cc(bb), {}^1S_0\text{-}\mathbf{6}]$, are considered for $\Xi_{cc(bb)}$ ($T_{cc(bb)}$) production; four bc-diquark configurations, $[bc, {}^3S_1\text{-}\bar{\mathbf{3}}]$, $[bc, {}^3S_1\text{-}\mathbf{6}]$, $[bc, {}^1S_0\text{-}\bar{\mathbf{3}}]$, and $[bc, {}^1S_0\text{-}\mathbf{6}]$, are taken into account for Ξ_{bc} production. The cross sections for each diquark configuration and the total cross sections versus transverse momentum and rapidity at the HL-LHC and

FCC are given. The cross section for doubly charmed tetraquark T_{cc} is also estimated.

Numerical results show that the cross section for $[cc, {}^3S_1\text{-}\bar{\mathbf{3}}]$ diquark is around 20–30 times the $[cc, {}^1S_0\text{-}\mathbf{6}]$ diquark for photon-photon fusion; the ratio decreases to 11–12 for photon-gluon fusion. Based on designed luminosities of each ion-ion collision at the HL-LHC and FCC, a considerable number of doubly charmed baryons and tetraquarks can be expected. Because the event topologies for ultraperipheral collision are very clear, the background from various QCD interactions can be suppressed; hence,

the detailed experimental investigation for Ξ_{cc} and T_{cc} is feasible. The transverse momentum and rapidity distributions are given. The productions for $\Xi_{bc/bb}$ are also discussed, leaving only a slight possibility for observing Ξ_{bc} through photon-gluon fusion at the FCC.

ACKNOWLEDGMENTS

[1] R. Aaij *et al.* (LHCb Collaboration), Phys. Rev. Lett. **119,** 112001 (2017).

[2] R. Aaij *et al.* (LHCb Collaboration), Phys. Rev. Lett. **121,** 162002 (2018).

[3] R. Aaij *et al.* (LHCb Collaboration), Phys. Rev. Lett. **121,** 052002 (2018).

[4] R. Aaij *et al.* (LHCb Collaboration), Nat. Phys. **18,** 751 (2022).

[5] G. T. Bodwin, E. Braaten, and G. P. Lepage, Phys. Rev. D **51,** 1125 (1995); **55,** 5853(E) (1997).

[6] A. F. Falk, M. E. Luke, M. J. Savage, and M. B. Wise, Phys. Rev. D **49,** 555 (1994).

[7] S. P. Baranov, Phys. Rev. D **54,** 3228 (1996).

[8] A. V. Berezhnoy, V. V. Kiselev, and A. K. Likhoded, Phys. At. Nucl. **59,** 870 (1996).

[9] M. A. Doncheski, J. Steegborn, and M. L. Stong, Phys. Rev. D **53,** 1247 (1996).

[10] A. V. Berezhnoy, A. K. Likhoded, and M. V. Shevlyagin, Phys. Lett. B **342,** 351 (1995).

[11] A. V. Berezhnoy, V. V. Kiselev, and A. K. Likhoded, Z. Phys. A **356,** 89 (1996).

[12] A. V. Berezhnoy, V. V. Kiselev, A. K. Likhoded, and A. I. Onishchenko, Phys. Rev. D **57,** 4385 (1998).

[13] J. P. Ma and Z. G. Si, Phys. Lett. B **568,** 135 (2003).

[14] J. Jiang, X. G. Wu, Q. L. Liao, X. C. Zheng, and Z. Y. Fang, Phys. Rev. D **86,** 054021 (2012).

[15] J. Jiang, X. G. Wu, S. M. Wang, J. W. Zhang, and Z. Y. Fang, Phys. Rev. D **87,** 054027 (2013).

[16] G. Chen, X. G. Wu, Z. Sun, Y. Ma, and H. B. Fu, J. High Energy Phys. 12 (2014) 018.

[17] X. J. Zhan, X. G. Wu, and X. C. Zheng, Phys. Rev. D **108,** 074030 (2023).

[18] H. Y. Bi, R. Y. Zhang, X. G. Wu, W. G. Ma, X. Z. Li, and S. Owusu, Phys. Rev. D **95,** 074020 (2017).

[19] Z. Sun and X. G. Wu, J. High Energy Phys. 07 (2020) 034.

[20] C. H. Chang, C. F. Qiao, J. X. Wang, and X. G. Wu, Phys. Rev. D **73,** 094022 (2006).

[21] C. H. Chang, J. P. Ma, C. F. Qiao, and X. G. Wu, J. Phys. G **34,** 845 (2007).

[22] P. H. Zhang, L. Guo, X. C. Zheng, and Q. W. Ke, Phys. Rev. D **105,** 034016 (2022).

[23] X. Luo, H. B. Fu, and H. J. Tian, Chin. Phys. C **47,** 053102 (2023).

[24] J. J. Niu, L. Guo, H. H. Ma, and X. G. Wu, Eur. Phys. J. C **79,** 339 (2019).

[25] J. J. Niu, L. Guo, H. H. Ma, X. G. Wu, and X. C. Zheng, Phys. Rev. D **98,** 094021 (2018).

[26] Y. q. Chen and S. z. Wu, Phys. Lett. B **705,** 93 (2011).

[27] T. Hyodo, Y. R. Liu, M. Oka, K. Sudoh, and S. Yasui, Phys. Lett. B **721,** 56 (2013).

[28] X. L. Hua, Y. Y. Li, Q. Wang, S. Yang, Q. Zhao, and B. S. Zou, arXiv:2310.04258.

[29] G. Baur, K. Hencken, D. Trautmann, S. Sadovsky, and Y. Kharlov, Phys. Rep. **364,** 359 (2002).

[30] C. A. Bertulani, S. R. Klein, and J. Nystrand, Annu. Rev. Nucl. Part. Sci. **55,** 271 (2005).

[31] A. J. Baltz, G. Baur, D. d'Enterria, L. Frankfurt, F. Gelis, V. Guzey, K. Hencken, Y. Kharlov, M. Klasen, S. R. Klein, and S Klein, Phys. Rep. **458,** 1 (2008).

[32] C. Li, J. Zhou, and Y. J. Zhou, Phys. Lett. B **795,** 576 (2019).

[33] C. Li, J. Zhou, and Y. J. Zhou, Phys. Rev. D **101,** 034015 (2020).

[34] X. Yao and B. Müller, Phys. Rev. D **97,** 074003 (2018).

[35] C. F. von Weizsacker, Z. Phys. **88,** 612 (1934).

[36] E. J. Williams, Phys. Rev. **45,** 729 (1934).

[37] R. N. Cahn and J. D. Jackson, Phys. Rev. D **42,** 3690 (1990).

[38] S. Knapen, T. Lin, H. K. Lou, and T. Melia, Phys. Rev. Lett. **118,** 171801 (2017).

[39] G. T. Bodwin and A. Petrelli, Phys. Rev. D **66,** 094011 (2002); **87,** 039902(E) (2013).

[40] A. De Rujula, H. Georgi, and S. L. Glashow, Phys. Rev. D **12,** 147 (1975).

[41] R. L. Jaffe, *The Gregory Breit Centennial Symposium* (World Scientific, Singapore, 2001).

[42] T. Hahn, Comput. Phys. Commun. **140,** 418 (2001).

[43] R. Mertig, M. Bohm, and A. Denner, Comput. Phys. Commun. **64,** 345 (1991).

[44] F. Feng and R. Mertig, arXiv:1212.3522.

[45] T. Hahn, Comput. Phys. Commun. **168,** 78 (2005).

[46] E. Bagan, H. G. Dosch, P. Gosdzinsky, S. Narison, and J. M. Richard, Z. Phys. C **64,** 57 (1994).

[47] A. Buckley, J. Ferrando, S. Lloyd, K. Nordström, B. Page, M. Rüfenacht, M. Schönherr, and G. Watt, Eur. Phys. J. C **75**, 132 (2015).

[48] A. Kusina, T. Ježo, D. B. Clark, P. Duwentäster, E. Godat, T. J. Hobbs, J. Kent, M. Klasen, K. Kovařík, F. Lyonnet *et al.*, Eur. Phys. J. C **80**, 968 (2020).

[49] R. Bruce, D. d'Enterria, A. de Roeck, M. Drewes, G. R. Farrar, A. Giammanco, O. Gould, J. Hajer, L. Harland-Lang, J. Heisig *et al.*, J. Phys. G **47**, 060501 (2020).

[50] D. d'Enterria, M. Drewes, A. Giammanco, J. Hajer, E. Bratkovskaya, R. Bruce, N. Burmasov, M. Dyndal, O. Gould, I. Grabowska-Bold *et al.*, J. Phys. G **50**, 050501 (2023).

[51] A. Abada *et al.* (FCC Collaboration), Eur. Phys. J. Special Topics **228**, 755 (2019).

[52] A. Dainese, U. A. Wiedemann, N. Armesto, D. d'Enterria, J. M. Jowett, J. P. Lansberg, J. G. Milhano, C. A. Salgado, M. Schaumann, M. van Leeuwen *et al.*, arXiv:1605 .01389.

[53] H. S. Shao and D. d'Enterria, J. High Energy Phys. 09 (2022) 248.

[54] F. S. Yu, H. Y. Jiang, R. H. Li, C. D. Lü, W. Wang, and Z. X. Zhao, Chin. Phys. C **42**, 051001 (2018).

[55] R. Aaij *et al.* (LHCb Collaboration), J. High Energy Phys. 12 (2013) 090.

[56] S. Acharya *et al.* (ALICE Collaboration), Phys. Rev. D **105**, L011103 (2022).

[57] R. L. Workman *et al.* (Particle Data Group), Prog. Theor. Exp. Phys. **2022**, 083C01 (2022).